12-3-2019

Langerhans Cells Orchestrate the Protective Antiviral Innate Immune Response in the Lymph Node.

Eric B. Wong
Thomas Jefferson University; Pennsylvania State University College of Medicine

Brian Montoya
Thomas Jefferson University

Colby Stotesbury
Thomas Jefferson University

Maria Ferez
Thomas Jefferson University

Ren-Huan Xu
Fox Chase Cancer Center

See next page for additional authors

Article

Cell Reports

Langerhans Cells Orchestrate the Protective Antiviral Innate Immune Response in the Lymph Node

Graphical Abstract

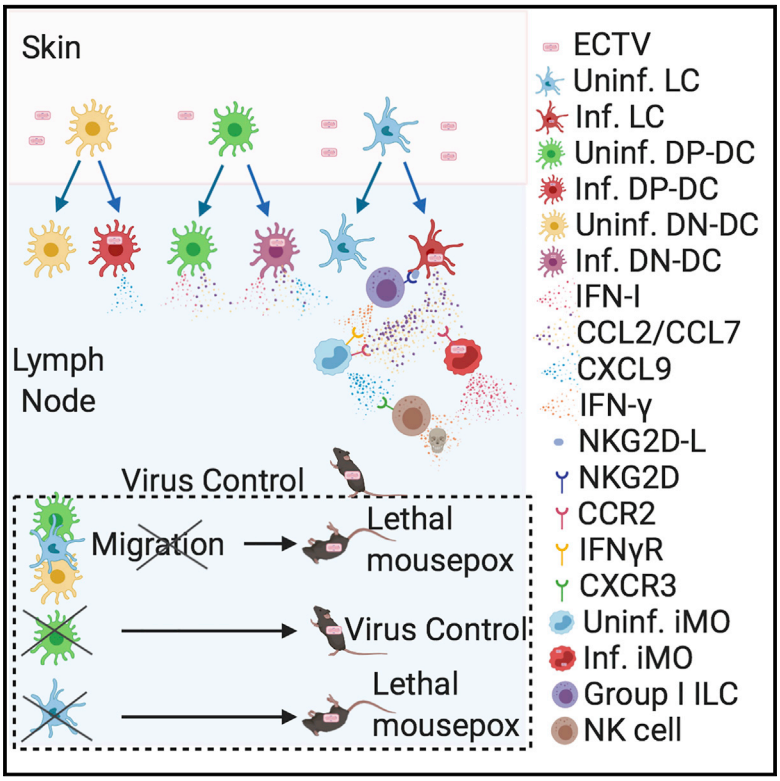

Highlights

- MHC class II^{hi} DCs migrate from the skin to the dLN to start the innate immune response
- MHC class II^{hi} DC subsets produce distinct cytokines according to their infection status
- LCs are required for iMO/NK cell migration to the dLN and resistance to mousepox

Authors

Eric Wong, Brian Montoya, Colby Stotesbury, Maria Ferez, Ren-Huan Xu, Luis J. Sigal

Correspondence

luis.sigal@jefferson.edu

In Brief

Wong et al. show that by producing chemokines that recruit monocytes and by upregulating NKG2D ligands that activate ILCs, Langerhans cells are responsible for the innate immune cascade in the lymph node that is critical for survival of infection with a disseminating virus.

Wong et al., 2019, Cell Reports *29*, 3047–3059
December 3, 2019
https://doi.org/10.1016/j.celrep.2019.10.118

CellPress

Cell Reports
Article

Langerhans Cells Orchestrate the Protective Antiviral Innate Immune Response in the Lymph Node

Eric Wong,[1] Brian Montoya,[1] Colby Stotesbury,[1] Maria Ferez,[1] Ren-Huan Xu,[2,3,4] and Luis J. Sigal[1,5,*]
[1]Department of Microbiology and Immunology, Thomas Jefferson University, BLSB 709 233 South 10th Street, Philadelphia, PA 19107, USA
[2]Immune Cell Development and Host Defense Program, Research Institute of Fox Chase Cancer Center, 333 Cottman Avenue, Philadelphia, PA 19111, USA
[3]Present address: Immunomic Therapeutics, Inc., Rockville, MD 20850, USA
[4]Present address: Renman Therapeutics, Gaithersburg, MD 20878, USA
[5]Lead Contact
*Correspondence: luis.sigal@jefferson.edu
https://doi.org/10.1016/j.celrep.2019.10.118

SUMMARY

During disseminating viral infections, a swift innate immune response (IIR) in the draining lymph node (dLN) that restricts systemic viral spread is critical for optimal resistance to disease. However, it is unclear how this IIR is orchestrated. We show that after footpad infection of mice with ectromelia virus, dendritic cells (DCs) highly expressing major histocompatibility complex class II (MHC class II^{hi} DCs), including CD207^{+} epidermal Langerhans cells (LCs), CD103^{+}CD207^{+} double-positive dermal DCs (DP-DCs), and CD103^{-}CD207^{-} double-negative dermal DCs (DN-DCs) migrate to the dLN from the skin carrying virus. MHC class II^{hi} DCs, predominantly LCs and DP-DCs, are the first cells upregulating IIR cytokines in the dLN. Preventing MHC class II^{hi} DC migration or depletion of LCs, but not DP-DC deficiency, suppresses the IIR in the dLN and results in high viral lethality. Therefore, LCs are the architects of an early IIR in the dLN that is critical for optimal resistance to a disseminating viral infection.

INTRODUCTION

Numerous viruses relevant to human and animal health use a lympho-hematogenous route of dissemination whereby they penetrate their hosts though disruptions of epithelial surfaces such as the skin, spread to the draining lymph nodes (dLNs) via afferent lymphatics, and become systemic by disseminating to the blood through efferent lymphatics (Flint et al., 2015). Yet, our mechanistic understanding of how the innate immune system of the host imposes protective barriers to the virus during lympho-hematogenous dissemination is incomplete, perhaps because few experimental models replicate this type of spread.

One of the best models to study lympho-hematogenous spread from the skin is ectromelia virus (ECTV), a member of the Orthopoxvirus genus of large, closely related DNA viruses and the causative agent of mousepox (the mouse homolog of human smallpox). In fact, ECTV was the virus used to elucidate this form of dissemination and is used as its archetype (Chapman et al., 2010; Flint et al., 2015; Virgin, 2005). Following infection through the skin of the footpad, ECTV disseminates lympho-hematogenously, resulting in high mortality in naive mice of susceptible strains, such as BALB/c, B6.D2-(D6Mit149-D6Mit15)/LusJ (B6.D2-D6) (Fang et al., 2011; Wallace and Buller, 1985; Wallace et al., 1985). On the other hand, naive young wild-type (WT) B6 mice and vaccinated BALB/c and B6.D2-D6 mice resist the infection with almost no signs of disease (Sigal, 2016). Our previous work using ECTV contributed to the now established paradigm that lymph nodes (LNs) are not only the organs where lymphocytes are primed before they egress to fight pathogens at primary sites of infection, but are also critical sites where innate and adaptive immune cells can restrict the spread of pathogens. For example, we and others have shown that natural killer (NK) cells in naive B6 mice (Fang et al., 2008; Jacoby et al., 1989; Parker et al., 2007) and memory CD8^{+} T cells in CD8-immunized BALB/c and B6.D2-D6 mice (Remakus et al., 2012; Xu et al., 2007) curb ECTV spread from the popliteal dLNs to the spleen and liver and protect from mousepox.

Others have further highlighted the importance of dLNs as restriction sites for pathogen dissemination, including subcapsular sinus macrophages limiting murine cytomegalovirus (MCMV) spread (Farrell et al., 2016) as well herpes simplex virus 1 (HSV-1) spreading unchecked to the brain due to a loss in dLN integrity (Conrady et al., 2010). Moreover, neutrophils are actively recruited to dLNs to phagocytose *Staphylococcus aureus* to prevent dissemination to blood and other organs (Bogoslowski et al., 2018). Furthermore, pathogens that can evade immune surveillance in the dLN have downstream consequences for the adaptive response. For example, the bluetongue virus in sheep increases dissemination by destroying follicular dendritic cells (DCs) in the LN, thus impairing B cell activation and antibody production (Melzi et al., 2016).

DCs, initially characterized for their expression of the integrin CD11c, are professional antigen-presenting cells (APCs) that are abundant in skin and other peripheral tissues, where they are strategically positioned to function as immune sentinels (Clausen and Stoitzner, 2015; Malissen et al., 2014). Skin DCs are a heterogeneous group of major histocompatibility complex class II (MHC class II^{hi}) cells that include epidermal CD103^{-}CD207^{+} Langerhans cells (LCs), CD103^{+}CD207^{+} double-positive dermal DCs (DP-DCs), which are part of

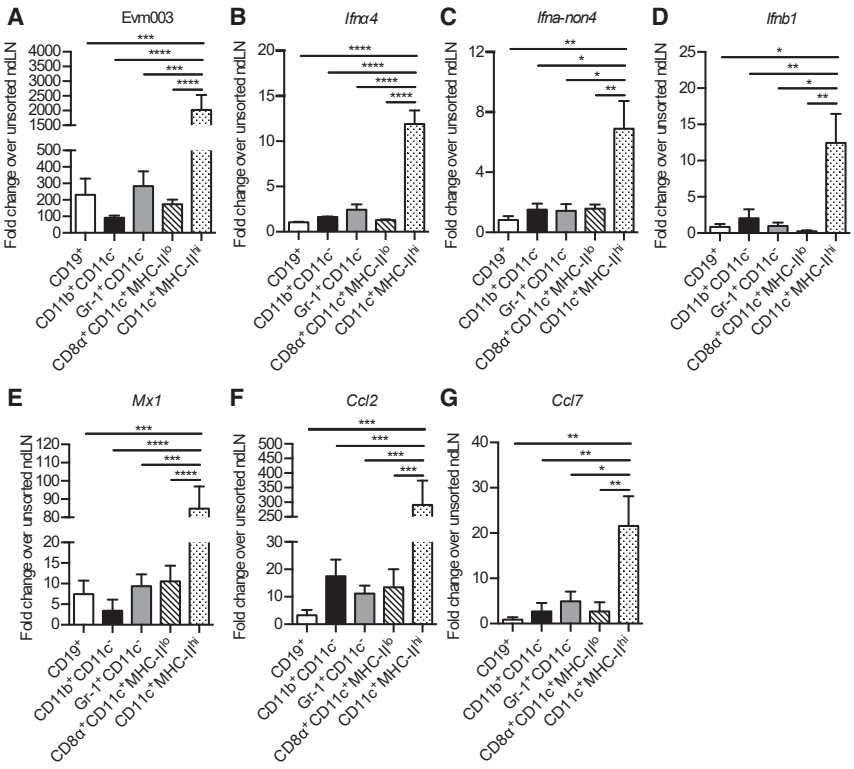

Figure 1. MHC Class II^{hi} DCs Mediate the Early IIR in the dLN after ECTV Infection

(A–G) Mice were infected in the footpad with 3,000 PFU ECTV. Data show expression of Evm003 (A), *Ifna4* (B), *Ifna-non4* (C), *Ifnb1* (D), *Mx1* (E), *Ccl2* (F), and *Ccl7*(G) in the specified sorted immune cell populations present in the dLN at 24 hpi. Data are displayed as mean ± SEM of pooled cells from six mice per group in one experiment, which is representative of two similar experiments. p values were calculated based on three technical replicates. For all, *p < 0.05, **p < 0.01, ***p < 0.001, and ****p < 0.0001. A complete gating strategy for MHC class II^{hi} DCs can be found in Figure S1.

the type 1 conventional DCs (cDC1), and CD103^{-}CD207^{-} double-negative dermal DCs (DN-DCs), which encompass the type 2 conventional DCs (cDC2) (Merad et al., 2008; Mildner and Jung, 2014; Murphy, 2013). Numerous inflammation/infection models, including contact hypersensitivity (Bennett et al., 2007), HSV-1 (Lee et al., 2009), lentivirus (He and Falo, 2006), leishmania (Moll et al., 1995), and *C. albicans* infection (Kashem et al., 2015), have demonstrated that skin DC subsets migrate to the dLN to prime T cell responses. In the case of footpad ECTV infection, we have previously shown that CD11c^{+} cells intrinsically expressing TLR9 and MyD88 produce CCL2 and CCL7 to recruit inflammatory monocytes (iMOs) to the dLN. At 60 h post-infection (hpi), many of these iMOs are infected and are the major producers of interferon I (IFN-I) (Xu et al., 2015), an antiviral cytokine that is critical for resistance to mousepox (Jacoby et al., 1989; Karupiah et al., 1993; Rubio et al., 2013; Xu et al., 2008). However, because CD11c is expressed by not only DCs but also other myeloid and lymphoid cells (Gordon and Taylor, 2005; Hume, 2008; Metlay et al., 1990), including iMOs, the specific CD11c^{+} cell responsible for iMO recruitment remained unknown. Recently, we have shown that at 24 hpi with ECTV, a population of DCs that express high levels of major histocompatibility complex class II molecules (MHC class II^{hi} DCs) upregulate NKG2D ligands to induce IFN-γ in group 1 innate lymphoid cells (G1-ILCs) already present in the dLN. This IFN-γ induces CXCL9 in uninfected iMO to further recruit circulating NK cells to the dLN which are critical for resistance to mousepox (Fang et al., 2011; Wong et al., 2018). Together, these data suggested that MHC class II^{hi} DCs may play an important role in the anti-viral innate immune response (IIR). However, whether infected and/or uninfected MHC class II^{hi} DCs migrate from the skin to the dLN after footpad ECTV infection remained to be demonstrated. More importantly, it remained unknown which subset of infected and/or uninfected skin DCs may play a role in orchestrating the IIR in the dLN, in the control of virus spread, and in resistance to viral disease. Here, we address these issues by showing that three types of MHC class II^{hi} DCs migrate to the dLN in response to ECTV infection and that the three MHC class II^{hi} DC subsets are functionally distinct in terms of cytokine production, with DP-DCs and LCs being much more pro-inflammatory than DN-DCs. We also show that LCs, but not DP-DCs, are required for iMO and NK cell recruitment to the dLN and their subsequent expression of IFN-I and IFN-γ. Moreover, we demonstrate that LCs but not DP-DCs are critical for virus control and intrinsic resistance to lethal mousepox.

RESULTS

MHC Class II^{hi} DCs Mediate the Early IIR in the dLN after ECTV Infection

To further understand the role of MHC class II^{hi} DCs (also CD45^{+}CD11c^{+}CD4^{-}CD8^{-}NK1.1^{-}CD64^{-}; Figure S1) in the initiation of the IIR in the dLN, we infected B6 mice in the footpad to mimic natural infection (3,000 plaque-forming units [PFUs] in 30 μL PBS) and sorted MHC class II^{hi} DCs and other immune cell subsets (gating strategy for sorting shown in Figure S1) present in the dLN at 24 hpi, isolated their RNA, and used qRT-PCR to determine infection by measuring mRNA for the ECTV gene *evm003* and activation status by measuring mRNA for IFN-I, the interferon-stimulated gene (ISG) *Mx1,* and the chemokines *Ccl2* and *Ccl7*, which are important for iMO recruitment (Xu et al., 2015). The results showed that MHC class II^{hi} DCs had significantly higher levels of all these transcripts (Figures 1A–1G), suggesting that MHC class II^{hi} DCs are the first to become infected and initiate the early anti-viral IIR in the dLN, and they might be responsible for iMO recruitment.

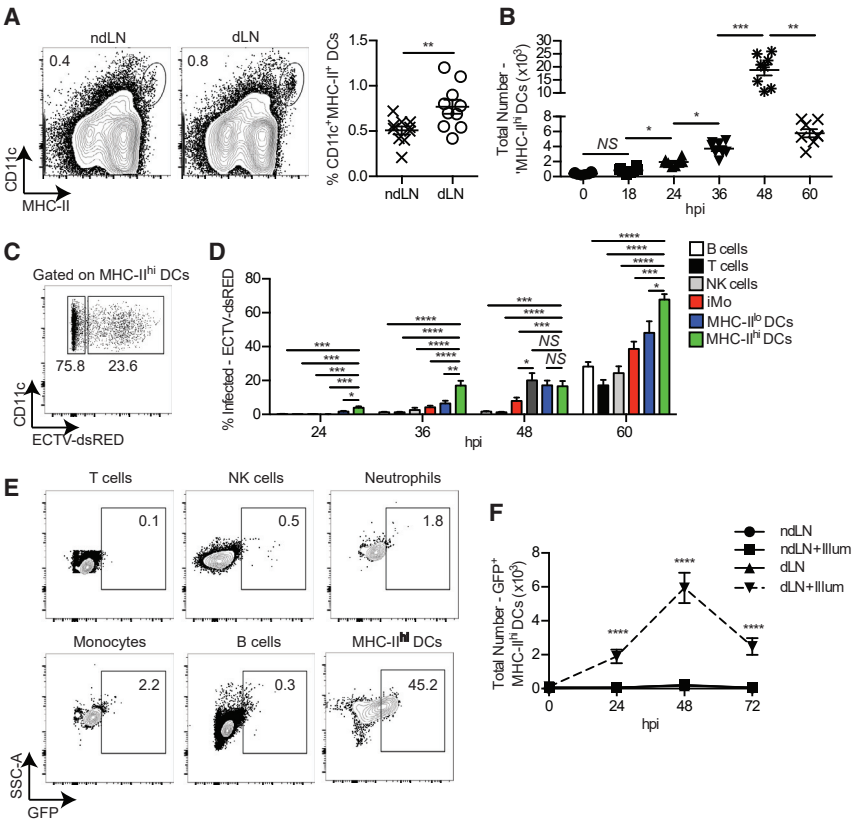

Figure 2. MHC Class II^{hi} DCs Migrate from the Skin to the dLN in Response to Infection

(A) Representative flow cytometry plots of gated CD11c^{+}MHC class II^{hi} DCs from the dLN at 24 hpi (left) and a graph displaying the range of frequencies are shown.

(B) Calculated number of MHC class II^{hi} DCs in the dLNs at the indicated time points post infection. Data are displayed as the mean ± SEM of eight mice per group combined from two independent experiments.

(C) Representative flow cytometry plot displaying ECTV infected (dsRED^{+}) and uninfected (dsRED^{-}) MHC class II^{hi} DCs at 48 hpi.

(D) Graph depicting the kinetics of infected (dsRED^{+}) cells in different immune cell populations. Data are displayed as the mean ± SEM of 12–14 mice per group combined from three independent experiments.

(E) Representative flow cytometry of different immune cell populations showing GFP^{+} gates at 48 hpi in dLNs from *Ubc*-PA-GFP mice that had been illuminated in the footpad with a 415-nm light 4 h before infection.

(F) Graph depicting the total number of GFP^{+} MHC class II^{hi} DCs at different time points in the indicated LNs of *Ubc*-PA-GFP mice whose feet had had been illuminated (illum) or not 4 h before infection. Additional controls for *Ubc*-PA-GFP mice are shown in Figure S2. p values are compared to non-illuminated ndLNs. Additional controls for Ubc-PA-GFP mice are shown in Figure S2. Data are displayed as the mean ± SEM of 12 mice per group combined from three independent experiments.

For all, *p < 0.05, **p < 0.01, ***p < 0.001, and ****p < 0.0001.

MHC Class II^{hi} DCs Migrate from the Skin to the dLN in Response to Infection

Compared to the contralateral non-draining LN (ndLN), the frequency (Figure 2A) of MHC class II^{hi} DCs was significantly increased in the dLN at 24 hpi, suggesting that infected MHC class II^{hi} DCs are rapidly recruited into the dLN following viral infection. According to kinetics analysis, their absolute numbers significantly increased in the dLN at 24 h, peaked at 48 h, and decreased by 60 hpi (Figure 2B). Infection with ECTV-dsRED revealed a significant fraction of MHC class II^{hi} DCs were infected at 48 hpi, similar to what was observed in iMOs (Figure 2C; et al., 2015). An analysis of the kinetics of infection in the dLN revealed that compared to other immune cell types, MHC class II^{hi} DCs are among the earliest cell types infected (24 and 36 h) and are the highest infected at later time points (60 h) (Figure 2D).

It was likely that these MHC class II^{hi} DCs migrated to the dLN from the skin, because it is known that MHC class II^{hi} DCs from the skin migrate to LNs at steady state and increase their migration during inflammation (Alvarez et al., 2008; Merad et al., 2008). To test this directly, we illuminated the footpads of mice transgenic for ubiquitously expressed photoactivatable GFPs (*Ubc*-PA-GFP mice; Victora et al., 2010) with a 415-nm light, and 4 h later, we infected them or not with ECTV. Under these conditions, any GFP^{+} cells present in the dLN at various times post-infection should have been in the skin during illumination (Figure S2). At 48 hpi, GFP^{+} cells represented a large proportion of the MHC class II^{hi} DCs in the dLN but were absent in other cell populations (Figures 2E and S2). This demonstrates that MHC class II^{hi} DCs, but not other cells, migrate from the skin to the dLN in responses to ECTV infection. Kinetic analysis showed that GFP^{+} MHC class II^{hi} DCs were detectable in dLNs at 24 hpi, peaked at 48 hpi, and decreased by 60 hpi (Figure 2F).

MHC Class II^{hi} DC Migration from the Skin to the dLN Is Required for iMO and NK Cell Accumulation in the dLN and Resistance to Lethal Viral Disease

It is well established that the migration of DCs to LNs requires G-protein-coupled receptor signaling (Alvarez et al., 2008; Tiberio et al., 2018) and that pertussis toxin (PT) inhibits G-protein-coupled-receptor-dependent cell migration (Burns, 1988; Karimian et al., 2012). To test whether the migration of MHC class II^{hi} DCs from the skin of the footpad to the dLN is required for antiviral defense, we administered PT directly into the same footpad (PT + ECTV mice) 24 h before and after ECTV and compared the IIR in their dLNs with the dLNs of mice receiving only ECTV (ECTV mice). Significantly fewer MHC class II^{hi} DCs accumulated in the dLN of PT + ECTV mice compared to the dLN of ECTV mice. Indeed, the number of MHC class II^{hi} DCs in the dLN of PT + ECTV mice was not

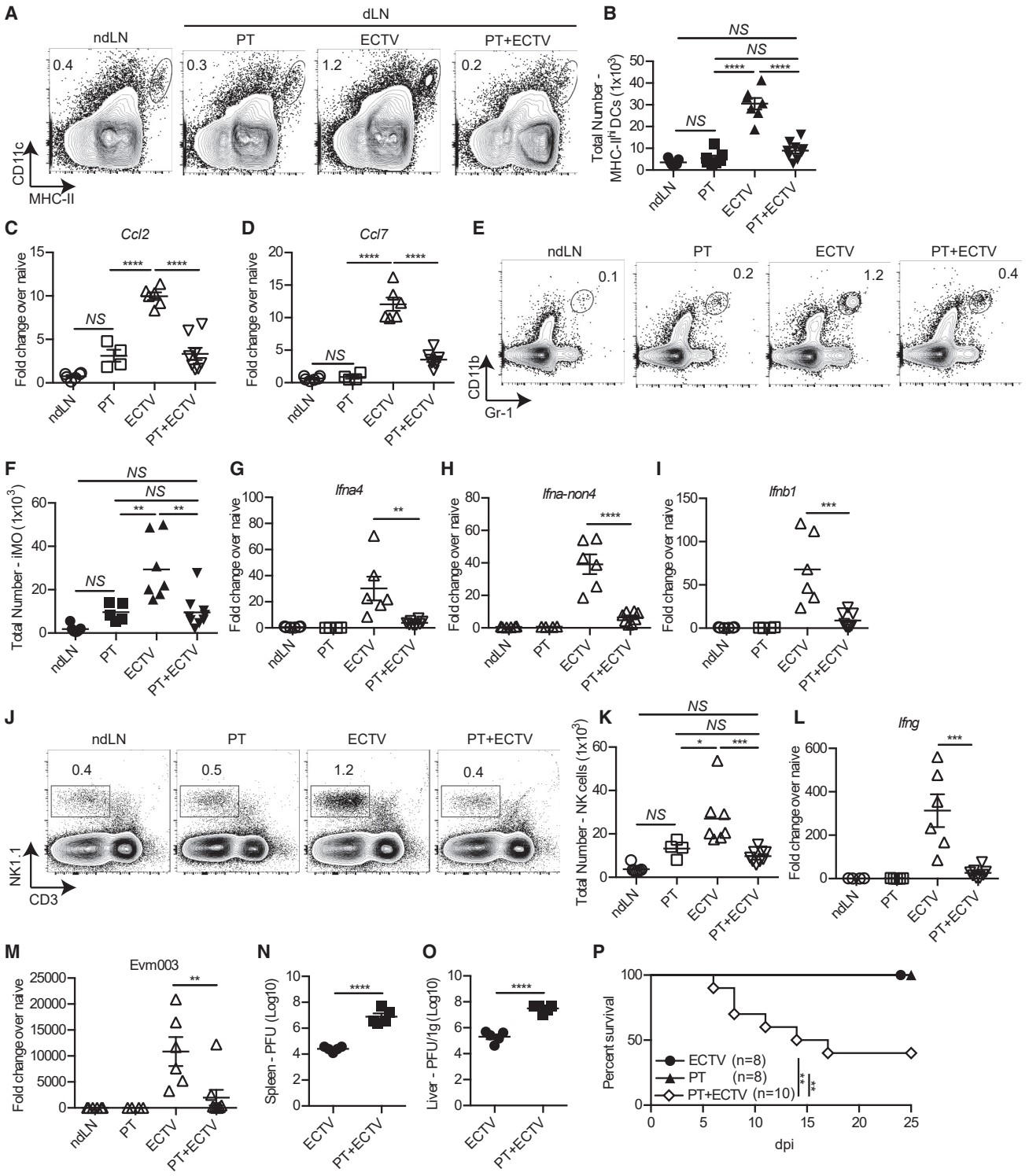

Figure 3. MHC Class II^{hi} DC Migration from the Skin to the dLN Is Required for iMO and NK Cell Accumulation and Resistance to Lethal Viral Disease

(A) Representative flow cytometry plots of MHC class II^{hi} DC frequency in the dLNs at 48 hpi with or without localized pertussis toxin (PT) administration in the footpad 24 h before and after infection.

(B) Calculated number of MHC class II^{hi} DCs from the dLNs of PT-treated mice at 48 hpi.

(legend continued on next page)

statistically different than those in the ndLNs of ECTV mice and dLNs of control mice that received only PT (Figures 3A and 3B). The decreased accumulation of MHC class II^{hi} DCs in the dLN of PT + ECTV mice was not due to a systemic effect of PT, because when PT and ECTV were administered in the right foot and only ECTV in the left foot, MHC class II^{hi} DC accumulation was curtailed in the right dLN, but not in the left dLN (Figure S3). Compared to ECTV mice, the dLN of PT + ECTV mice also had significantly decreased transcription of *Ccl2* (Figure 3C) and *Ccl7* (Figure 3D), which are required for iMO recruitment, significantly diminished iMO accumulation (Figures 3E and 3F) and significantly reduced transcription of all IFN-I subtypes (Figures 3G–3I). Furthermore, PT + ECTV mice had significantly diminished frequency (Figure 3J) and total numbers (Figure 3K) of NK cells and consequently significantly decreased levels of IFN-γ expression in the dLN (Figure 3L). Notably, while PT + ECTV mice transcribed significantly less viral RNA in the dLN at 2 dpi than ECTV mice (Figure 3M), viral loads at 7 dpi in the spleen (Figure 3N) and liver (Figure 3O) were significantly higher in PT + ECTV mice than in ECTV mice. Moreover, even though B6 mice are naturally resistant to lethal mousepox, a significant proportion of PT + ECTV mice succumbed to the infection (Figure 3P). These data indicate that G-protein-coupled-receptor-dependent MHC class II^{hi} DC migration to the dLN plays a crucial role in the early transport of ECTV to the dLN and that this process is crucial for protective innate immunity in the dLN and resistance to viral disease.

The Three Major Subsets of Skin DCs Migrate to the dLN in Response to ECTV Infection

We next compared the effects of ECTV infection in the three subsets of skin-derived MHC class II^{hi} DCs in the dLN: LCs (CD103^{-}CD207^{+}), DP-DCs (CD103^{+}CD207^{+}), and DN-DCs (CD103^{-}CD207^{-}). The frequency of DN-DCs and DP-DCs significantly increased while LC frequency concomitantly decreased after infection at 48 h (Figures 4A and 4B). However, the total numbers of the three skin-DC subsets in the dLN were significantly increased at 48 hpi (Figure 4C). A kinetics analysis using *Ubc*-PA-GFP mice demonstrated that the three DC subsets followed a similar rate of migration, initially arriving to the dLN at 24 hpi, peaking at 48 hpi, and precipitously dropping by 60 hpi (Figures 4D and S4). Infection with ECTV-dsRED revealed a differential rate of infection among the DC subsets, with DP-DCs having the highest frequency of infected cells (Figures 4E and S4). Moreover, while a considerable fraction of GFP^{+} cells of the three MHC class II^{hi} subsets were infected (dsRED^{+}), many were uninfected (dsRED^{-}) at all times tested (Figure 4E). This suggests that viral-induced inflammation promotes the migration to the dLN of infected and also noninfected cells of the three skin-derived MHC class II^{hi} DC subsets. Furthermore, infected, but not uninfected, MHC class II^{hi} DCs significantly upregulated NKG2D ligand MULT-1 expression, indicating that all three subsets are capable of mediating the early IFN-γ response from ILCs in the LN (Figures 4F and 4G).

MHC Class II^{hi} DC Subsets Respond Differently to Viral Infection

Next, we investigated whether the three subsets of MHC class II^{hi} DCs have similar or distinct cytokine profiles in response to infection and whether this is affected by their infection status. With this purpose, we infected B6 mice with ECTV-dsRED; sorted infected (dsRED^{+}) and uninfected (dsRED^{-}) DN-DCs, DP-DCs, and LCs from the dLN; and quantified transcripts for the viral gene Evm003, IFN-Is, and various cytokines and chemokines. As expected, dsRED^{+} MHC class II^{hi} of all subsets transcribed significantly higher amounts of viral RNA than their dsRED^{-} counterparts, yet DN-DCs transcribed significantly more viral RNA than LCs and DP-DCs (Figure 5A). Conversely, compared to DN-DCs, infected DP-DCs and LCs transcribed higher levels of mRNA for most cytokines and chemokines, including *Ccl2* (Figure 5B), which is required for the recruitment of iMOs. An exception was *Ccl7*, also required for iMO recruitment, whose mRNA was transcribed highest by uninfected DP-DCs (Figure 5C). *Cxcl9* was transcribed mostly by infected cells (Figure 5D). Other cytokine/chemokine mRNAs varied in the level of transcription between MHC class II^{hi} subsets with infected DP-DCs and LCs expressing high levels of mRNA for *Ccl8* (also in uninfected DP-DCs), *Ccl19* (also in uninfected LCs), *Il1b* (also in uninfected LCs), *Il6*, *Il17*, *Il18*, and *Tnf* (Figures 5E–5K). In the case of IFN-I mRNA, *Ifnb1* (Figure 5L), *Ifna4* (Figure 5M), and *Ifna-non4* (Figure 5N) were upregulated by the three subsets of infected DCs to different levels, while the cells that mostly upregulated *Ifna-non4* were uninfected DP-DCs.

(C and D) Expression of *Ccl2* (C) and *Ccl7* (D) in the dLNs of the indicated mice at 48 hpi as determined by qRT-PCR. Data are displayed as mean ± SEM from four to six mice per group in one experiment, which is representative of three similar experiments.
(E) Representative flow cytometry plots of iMOs in the dLN at 48 hpi.
(F) Calculated numbers of iMOs in the dLN at 48 hpi. Data are displayed as the mean ± SEM of five to nine mice per group combined from three independent experiments.
(G–I) As in (C) and (D), but measuring RNA for *Ifna4* (G), *Ifna-non4* (H), and *Ifnb1* (I). Data are displayed as mean ± SEM from five to eight mice per group in one experiment, which is representative of two similar experiments.
(J) Representative flow cytometry plots of NK cells in the dLNs at 48 hpi.
(K) Calculated numbers of NK cells in the dLN at 48 hpi. Data are displayed as the mean ± SEM of five to nine mice per group combined from three independent experiments.
(L and M) As in (C) and (D) but measuring IFN-γ (L) and Evm003 (M). Data are displayed as mean ± SEM from four to six 6 mice per group in one experiment, which is representative of three similar experiments.
(N and O) Virus loads in the spleen (N) and livers (O) of the indicated mice at 7 dpi as determined by plaque assay. Data are displayed as the mean ± SEM of five mice per group.
(P) Survival of indicated mice.
For all, *$p < 0.05$, **$p < 0.01$, ***$p < 0.001$, and ****$p < 0.0001$. Additional controls for the effects of PT inoculation are depicted in Figure S3.

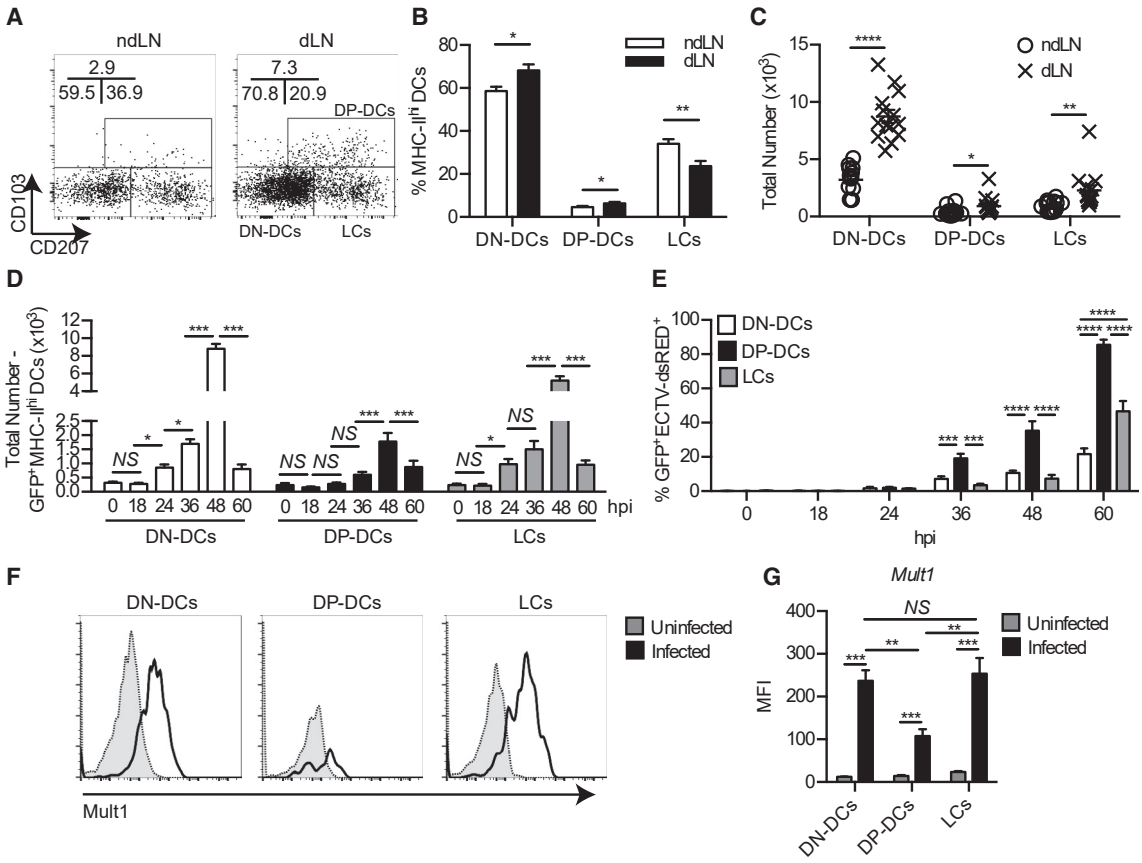

Figure 4. The Three Major Subsets of Skin DCs Migrate to the dLN in Response to ECTV Infection

(A) Gating strategy and representative flow cytometry plots for MHC class II^{hi} DC subsets at 48 hpi.

(B and C) Graph depicting the frequency (B) and calculated total numbers (C) of MHC class II^{hi} DC subsets in the dLNs at 48 hpi. An additional gating strategy is depicted in Figure S4. Data are displayed as mean ± SEM from 12–14 mice per group, combined from three similar independent experiments.

(D) Graph depicting the calculated total number of GFP + MHC class II^{hi} DCs at the indicated time points in the dLNs of *Ubc*-PA-GFP mice whose feet had been illuminated 4 h before infection. Data are displayed as mean ± SEM from 10 mice per group, combined from two similar independent experiments.

(E) Graph depicting the frequency of ECTV-dsRED^{+}GFP^{+}MHC class II^{hi} DC subsets at the indicated time points in the dLN of the mice in (D). Data, displayed as mean ± SEM, correspond to 15 mice per group, combined from three similar independent experiments. Complete gating strategies are depicted in Figure S4.

(F and G) Representative histograms (F) and graph (G) depicting the MFI of NKG2D ligand Mult1 in MHC class II^{hi} DC subsets. Data, displayed as mean ± SEM, correspond to 10 mice per group, combined from two similar independent experiments.

For all, *p < 0.05, **p < 0.01, ***p < 0.001, and ****p < 0.0001.

LCs, but Not DP-DCs, Are Required for Optimal Resistance to ECTV Infection

Given their different functionality and highly induced proinflammatory cytokine profiles, we next investigated whether DP-DCs and/or LCs are required for the early IIR in the dLN and resistance to lethal mousepox. We tested the role of DP-DCs using *Batf3*$^{-/-}$ mice, which lack DP-dermal DCs and also LN resident CD8α^{+} DCs (Hildner et al., 2008). Compared to WT B6 mice, *Batf3*$^{-/-}$ mice infected with ECTV had no significant differences in the frequency of total MHC class II^{hi} DCs (Figure 6A) but had a significant reduction in DP-DCs in the dLN, while DN-DCs and LCs were not affected (Figure 6B). The lack of DP-DCs did not affect the overall transcription levels of *Ccl2* (Figure 6C) or *Ccl7* (Figure 6D), the accumulation of iMOs (Figure 6E), or the subsequent transcription of IFN-I genes (Figure 6F–6H) in the dLN. Similarly, the frequency of NK cells (Figure 6I) and IFN-γ mRNA in the dLN (Figure 6J) of *Batf3*$^{-/-}$ mice did not differ compared to B6 mice. Moreover, WT B6 and *Batf3*$^{-/-}$ mice had comparable levels of viral RNA transcription in the dLN at 48 hpi (Figure 6K) and no significant differences in viral loads at 7 dpi in both the spleen (Figure 6L) and liver (Figure 6M), and they were fully resistant to lethal mousepox (Figure 6N).

Next, we determined the role of LCs using mice transgenic for the human diphtheria toxin (DT) receptor driven by the human langerin (CD207) promoter (CD207-DTR mice, herein DTR^{+}), wherein administration of DT results in ablation of LCs, but not DP-DCs (Bobr et al., 2010; Kaplan, 2010; Kaplan et al., 2005). As expected, administration of DT to DTR^{+} mice, but not to DTR^{-} littermate controls, significantly decreased the accumulation of LCs (Figure 7A) but not of DN-DCs (Figure 7B) or DP-DCs (Figure 7C) in the dLN following ECTV infection. Furthermore, DT administration to DTR^{+} mice, but not to DTR^{-} mice, significantly

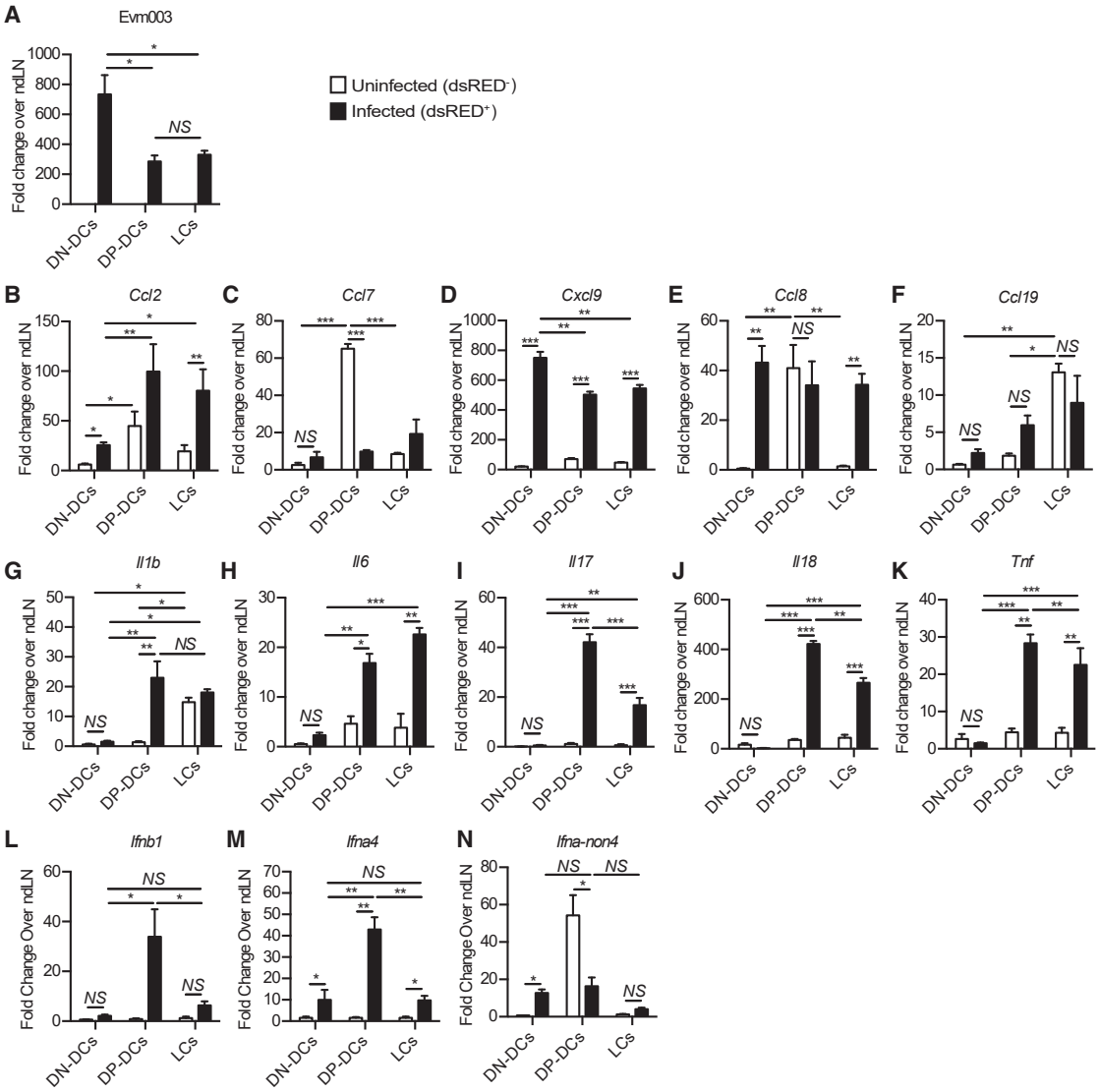

Figure 5. MHC Class II^{hi} DC Subsets Respond Differently to Viral Infection

(A–N) Expression of mRNA for EVM003 (A), the chemokines *Ccl2* (B), *Ccl7* (C), *Cxcl9* (D), *Ccl8* (E), and *Ccl19* (F); the inflammatory cytokines *Il1b* (G), *Il6* (H), *Il17* (I), *Il18* (J), and *Tnf* (K); and the IFN-I subtypes *Ifnb1* (L), *Ifna4* (M), and I*fna-non4* (N), in the different MHC class II^{hi} DC subsets distinguished by infection status in the dLN at 48 hpi. Data are displayed as mean ± SEM of pooled cells from eight mice per group in one experiment, which is representative of two similar experiments. p values were calculated based on three technical replicates. For all, *p < 0.05, **p < 0.01, ***p < 0.001, and ****p < 0.0001.

decreased the transcription of *Ccl2* (Figure 7D) and *Ccl7* (Figure 7E), and, likely as a consequence, the accumulation of iMOs (Figure 7F) and reduced IFN-I expression levels in the dLN (Figure 7G). Moreover, DTR^{+} mice, but not DTR^{-} mice, had a significant reduction in total NK cell numbers (Figure 7H) and IFN-γ expression in the dLN (Figure 7I). Furthermore, DTR^{+} mice, but not DTR^{-} mice, had a significant increase in viral RNA transcription in the dLN at 2 dpi (Figure 7J), significantly increased virus loads in the spleen (Figure 7K) and liver (Figure 7L) at 7 dpi, and significant mortality following ECTV infection (Figure 7M). Together, these data demonstrate that LCs, but not DP-DCs, are important for the CCL2/CCL7-dependent accumulation of iMOs that primarily mediates the IFN-I response, as well as facilitating NK cell accumulation and subsequent IFN-γ response in the dLN. Ultimately, this LC-mediated IIR is critical for optimal virus control and survival to mousepox.

DISCUSSION

We have previously shown that a highly choreographed IIR in the dLN is critical to curb systemic viral dissemination and resistance to mousepox through the antiviral functions of IFN-I and NK cells (Fang et al., 2011; 2008; Wong et al., 2018; Xu et al., 2015). In particular, we showed that after infection of the footpad with ECTV, CD11c^{+} cells (most likely DCs) are required for the CCL2/CCL7-mediated recruitment of iMOs into the dLN

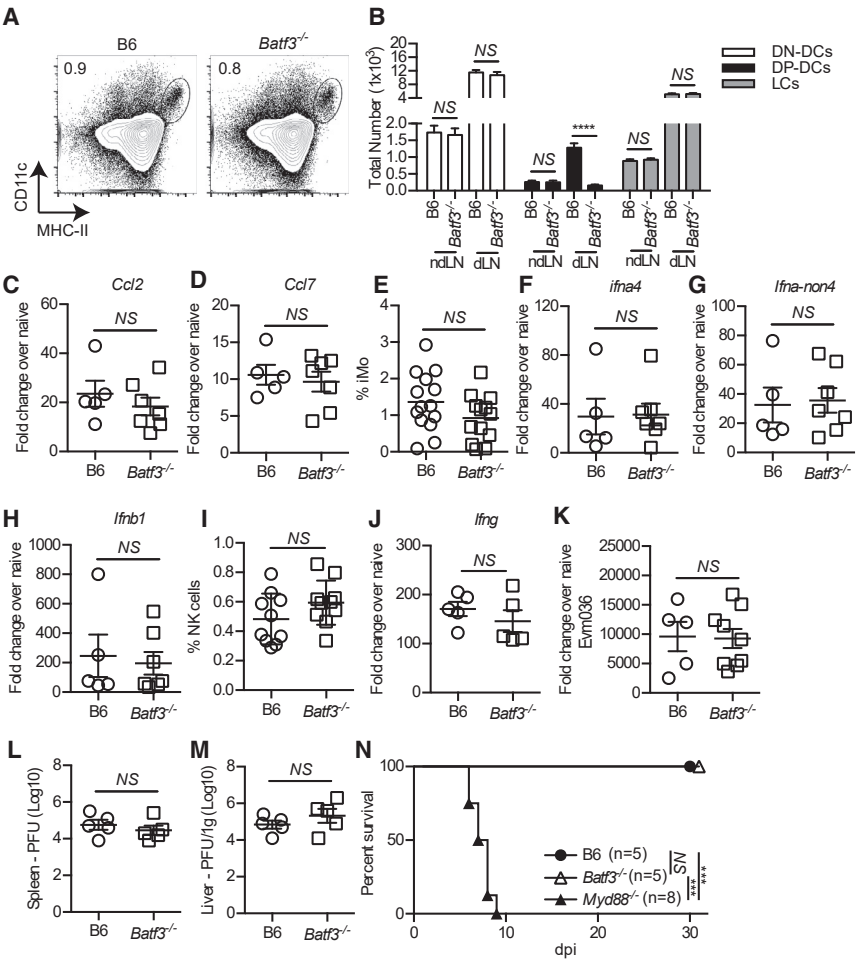

Figure 6. DP-DCs Are Not Required for an Efficient IIR in the dLN or Resistance to Lethal Mousepox

(A) Representative flow cytometry plots of MHC class II^{hi} DC frequency in the dLNs at 48 hpi in *Batf*$^{-/-}$ mice.

(B) Total number of DN-DCs, DP-DCs, and LCs in the dLNs of B6 and *Batf*$^{-/-}$ mice at 48 hpi.

(C and D) Expression of *Ccl2* (C) and *Ccl7* (D) in the dLNs at 48 hpi as determined by qRT-PCR. Data are displayed as mean ± SEM from five to seven mice per group in one experiment, which is representative of three similar experiments.

(E) Frequency of iMOs in the dLNs of B6 and *Batf*$^{-/-}$ mice 48 hpi.

(F–H) As in (C) and (D), but measuring expression of the IFN-I subtypes *Ifna4* (F), *Ifna-non4* (G), and *Ifnb1* (H) in the dLN at 48 hpi.

(I) Frequency of NK cells in the dLNs of B6 and *Batf*$^{-/-}$ mice 48 hpi.

(J and K) Expression of IFN-γ (J) and Evm036 (K) in the dLN at 48 hpi as determined by qRT-PCR. Data are displayed as mean ± SEM from five to eight mice per group in one experiment, which is representative of three similar experiments.

(L and M) Virus loads in the spleen (L) and livers (M) of the indicated mice at 7 dpi as determined by plaque assay.

(N) Survival of the indicated mice.

For all, *p < 0.05, **p < 0.01, ***p < 0.001, and ****p < 0.0001.

(Xu et al., 2015) and that MHC class II^{hi} DCs in the dLN, which are presumably skin derived (Malissen et al., 2014; Merad et al., 2008, 2013), upregulate the expression of NKG2D ligands to stimulate the production of IFN-γ in NK cells already in the dLN at the time of infection (Wong et al., 2018). The consequence of these processes, both requiring intrinsic TLR9/MyD88 in CD11c^{+} cells, is that infected iMOs produce IFN-I (Xu et al., 2015) and uninfected iMOs responding to IFN-γ produce CXCL9 to recruit circulating NK cells (Wong et al., 2018; Xu et al., 2015). We now show that as early as 24 hpi, MHC class II^{hi} DCs express 10-fold more ECTV transcripts than any other cell type in the dLN, suggesting that they are the first cells infected in the dLN. Concordantly, MHC class II^{hi} DCs express more transcripts for IFN-I and the ISG MX1, suggesting that they are the first cells that sense viral infection. Moreover, compared to other cell types, MHC class II^{hi} DCs express significantly more transcripts for CCL2 and CCL7. This suggests that MHC class II^{hi} DCs are the CD11c^{+} cells responsible for the recruitment of iMOs to the dLN and that in addition to their role in promoting adaptive immune responses through antigen presentation (Allan et al., 2006; Bedoui and Greyer, 2014; Helft et al., 2012; Waithman et al., 2013), MHC class II^{hi} DCs also play a pivotal role at assembling the IIR in the dLN. Of note, our results contrast with the findings in other viral models of footpad infection, where the first cells to become infected are subcapsular macrophages. Perhaps the difference is that because ECTV is a mouse pathogen that normally spreads from abrasions of the skin, we can use doses of only 3,000 PFU of virus, while other systems, including vesicular stomatitis virus (VSV) (Iannacone et al., 2010; Junt et al., 2007), modified vaccinia Ankara (MVA) (Garcia et al., 2012), and MCMV (Farrell et al., 2015), use doses of 10^6 to 5×10^6 PFUs, which may directly push viral particles into the LN bypassing the need for skin infection.

It is well established that skin DCs constitutively migrate to LNs, where they are detected as MHC class II^{hi} DCs, and that their migration is increased during inflammation (Clausen and Stoitzner, 2015; Malissen et al., 2014; Merad et al., 2013, 2008). However, whether ECTV infection in the footpad increases skin DC migration was not known. We found the frequency and total numbers of MHC class II^{hi} DCs in the dLN significantly increased starting at 24 hpi. Peak accumulation occurred at 48 hpi, which preceded the peak of iMO accumulation (60 hpi) (Xu et al., 2015), and then precipitously dropped in total numbers, leaving a large proportion of those remaining infected. This outcome suggests that the steep decline in MHC class II^{hi} DCs might be due to ECTV-induced cell death or their killing by iMOs or NK cells. Footpad illumination of *Ubc*-PA-EGFP transgenic mice (Victora et al., 2010) definitively confirmed that MHC class II^{hi} DCs migrate from the footpad to the dLN and that they are the only cell type that do so.

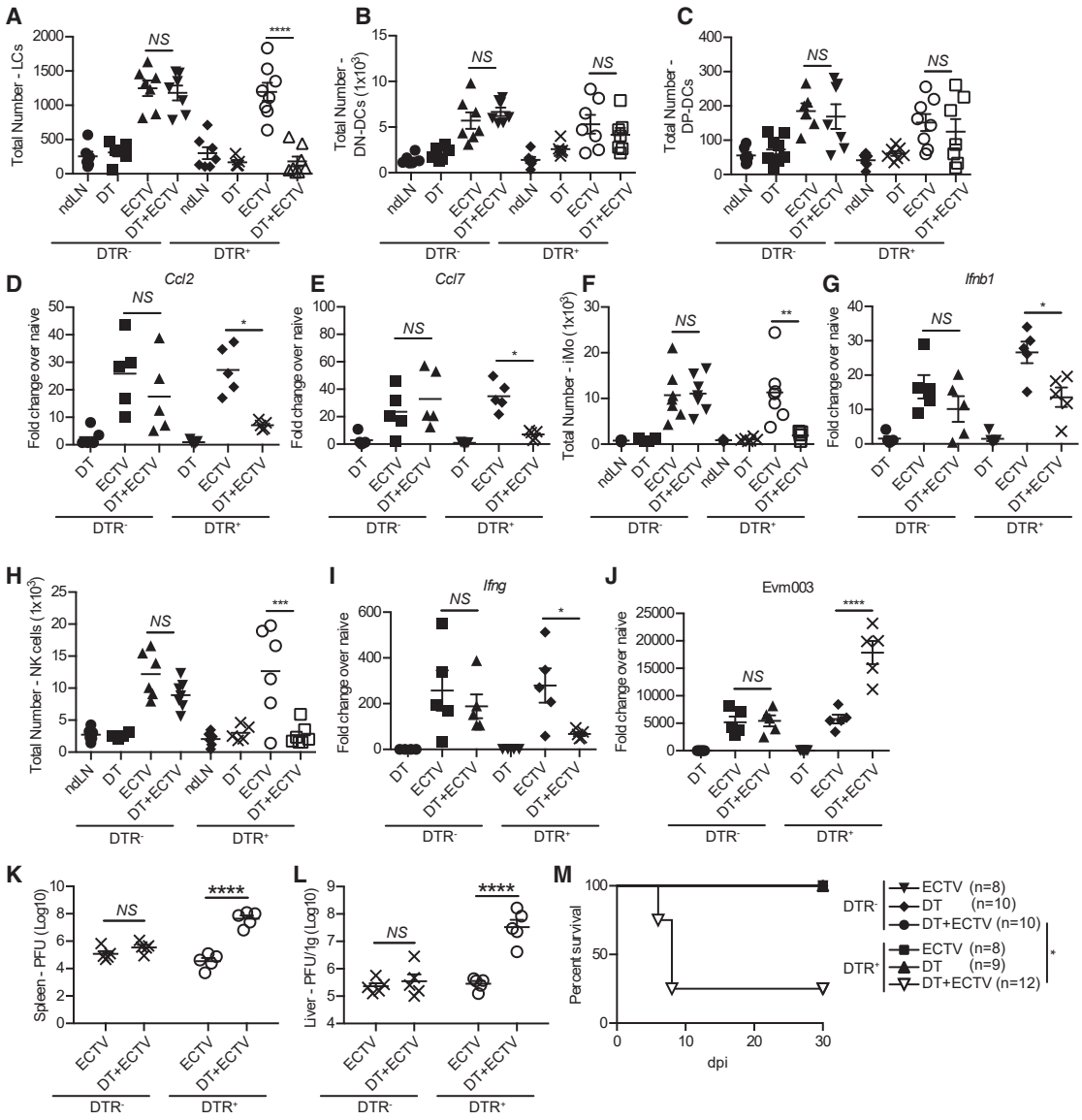

Figure 7. LCs Are Required for the Recruitment of iMOs to the dLN and Optimal Resistance to Lethal Mousepox

(A–C) Calculated numbers of LCs (A), DN-DCs (B), and DP-DCs (C) in the dLNs of DTR$^+$ mice and their littermate controls at 48 hpi and after prior DT treatment.

(D and E) Expression of *Ccl2* (D) and *Ccl7* (E) in the dLNs at 48 hpi as determined by qRT-PCR. Data are displayed as mean ± SEM from five mice per group in one experiment, which is representative of three similar experiments.

(F) Calculated number of iMOs in the dLN of the indicated mice at 48 hpi and after prior DT treatment.

(G) As in (D) and (E) but measuring *Ifnb1*.

(H) Calculated number of NK cells in the dLN of the indicated mice at 48 hpi and after prior DT treatment.

(I and J) As in (D) and (E) but measuring IFN-γ (I) and Evm003 (J).

(K and L) Virus loads in the spleen (K) and liver (L) of the indicated mice at 7 dpi as determined by plaque assay.

(M) Survival of the indicated mice.

For all, *p < 0.05, **p < 0.01, ***p < 0.001, and ****p < 0.0001.

The mechanisms and importance of MHC class II^{hi} DC migration from the skin to the dLN in virus control were revealed through the administration of PT in the footpad to block immune cell migration (Burns, 1988; Karimian et al., 2012). One caveat is that localized PT treatment in the footpad blocks all chemokine-dependent immune cell migration from the skin to the dLN; however, the data from the *Ubc*-PA-GFP mice indicate that it is overwhelmingly MHC class II^{hi} DCs that are traveling to the dLN after infection. PT-treated B6 mice had highly reduced accumulation of MHC class II^{hi} DCs in the dLN and had significantly reduced transcripts for the monocyte-recruiting chemokines CCL2 and CCL7 in the dLN. This correlated with reduced recruitment of

iMOs and decreased IFN-I transcripts in the dLN at 60 hpi. PT-treated mice also had significantly lower numbers of NK cells and reduced IFN-γ expression in the dLN, all of which resulted in increased viral loads in liver and spleen at 7 dpi, and high lethality. Paradoxically, at 2 dpi, viral transcripts in the dLNs of PT treated mice were significantly reduced. This suggests that at least the initial transport of virus to the dLN is mediated by MHC class II^{hi} DCs and that this is important to expedite the induction of a protective IIR.

When we identified the subpopulations of MHC class II^{hi} DCs as epidermal LCs, dermal DN-DCs, and DP-DCs, we found that they all migrate from the footpad to the dLN at equivalent rates. This is in contrast to previous studies that showed LCs lagging behind in their movement to the dLN after activation due to longer detachment times from keratinocytes (Fukunaga et al., 2008; Kissenpfennig et al., 2005; Stoitzner et al., 2002; West and Bennett, 2018). However, these studies utilized mechanical disruption of the skin or topical agents to induce inflammation and the migratory kinetics may differ from a viral infection, possibly due to activation of different sensing pathways. Of note, at all times, the three cell types differed in infection frequencies, with DP-DCs being the most infected, followed by LCs; the frequency of infected DN-DCs was relatively low. Furthermore, all three DC subsets upregulate Mult1 when infected, with DN-DCs and LCs expressing the highest levels, indicating their potential to induce IFN-γ from NK cells and ILCs already in the LN to recruit iMOs (Wong et al., 2018).

Broadly, the different MHC class II^{hi} subsets vary in their intrinsic and bystander response to infection, as determined by their expression of various genes, in the following ways: (1) Infected DN-DCs produce the most viral transcripts but lag behind LCs and DP-DCs in cytokine transcripts, except for *Ccl8* and *Cxcl9*, which they highly upregulate; (2) DN-DCs do not respond as bystanders, at least for the genes that we tested; (3) infected DP-DCs and LCs had a very proinflammatory profile, expressing high levels of *Il1b*, *Il6*, *Il17*, *Il18*, and *Tnf* mRNA (in general, these cells also transcribed various IFN-I genes and most of the chemokines genes tested); and (4) bystander DP-DCs and LCs in general responded less than their infected counterparts, with the exception that uninfected DP-DCs transcribed *Ccl7* and *Ifna-non4* very highly and uninfected LCs were as efficient as their infected counterparts at transcribing *Ccl19* and *Il1b*. Important to note, irrespective of their infection status, DP-DCs and LCs, but not DN-DCs, expressed mRNA for CCL2 and CCL7, which are necessary for iMO recruitment.

The finding that whether infected or bystander, MHC class II^{hi} DC subsets respond very differently is intriguing. Moreover, there are also interesting differences between iMO and MHC class II^{hi} DCs. For example, we have previously shown that bystander, but not infected, iMOs are major producers of *Cxcl9* (Wong et al., 2018), while here, we show that *Cxcl9* is expressed by infected, but not bystander, MHC class II^{hi} DCs. Also, we have shown that infected iMOs transcribe more RNA for all subtypes of IFN-I than uninfected iMOs and that the signaling pathway requires STING and IRF7 (Xu et al., 2015). While this remained true for *Ifnb1* and *Ifna4* in DP-DCs and LCs and also for *Ifna*-non4 in DN-DCs and LCs, the cells that mostly upregulated *Ifna-non4* were uninfected DP-DCs. This finding suggests that DP-DCs may use an alternative signaling mechanism to produce IFN-I non-a4, perhaps one that depends on TLR9 and MyD88. Together, this suggests that *in vivo*, the response to direct and bystander infection varies highly between cell types, which may be important for antiviral defense. RNA sequencing (RNA-seq) experiments could expand this finding and reveal clues about these cell-intrinsic roles depending on infection status.

Batf3$^{-/-}$ mice mounted an IIR that was similar to B6 controls and, as previously shown by others (Kaminsky et al., 2015), were fully resistant to mousepox. Of note, DP-DCs and also Batf3-depedent CD8α^{+} DCs are known to be the cells that cross-present peptide on MHC class I to CD8 T cells in LNs (Desai et al., 2018; Henri et al., 2010; Hildner et al., 2008; Torti et al., 2011). While the emphasis of this paper is focused on identifying the MHC class II^{hi} DC subset(s) required to initiate the early IIR in the dLN, it is important to mention that CD8^{+} T cells are essential for resistance to mousepox (Fang and Sigal, 2005), which raises the question of how CD8 T cells are initiated in *Batf3*$^{-/-}$ mice. Yet, we have also previously shown that cross-presentation is dispensable for the CD8 T cell response to vaccinia virus (Xu et al., 2010), which is highly related to ECTV. Moreover, others have shown that during ECTV infection, the majority of peptide-MHC class I is presented by infected cells, and that *Batf3*$^{-/-}$ mice mount normal CD8 T cell responses to ECTV (Kaminsky et al., 2015; Sei et al., 2015) strongly suggesting that direct and not cross-presentation is also the main mechanism of CD8 T cell priming during ECTV infection. One possible caveat with *Batf3*$^{-/-}$ mice is that interleukin-12 (IL-12) can restore DP DCs (Tussiwand et al., 2012) and IL-12 is modestly induced during ECTV infection. Yet, recovery of DP-DCs is unlikely to explain our results, because we demonstrated the absence of DP-DCs in *Batf3*$^{-/-}$ mice at the times when IIRs were normal.

A significant result of our study is the finding that LCs, but not DP-DCs, are required for optimal IIRs in the dLN and resistance to mousepox. These results expand our previous study showing that CCL2 and CCL7 produced by CD11c^{+} cells are primarily responsible for the recruitment of iMOs to the dLN and the subsequent IFN-I response (Xu et al., 2015). Even though both DP-DCs and LCs showed significantly high levels of proinflammatory cytokine profiles, particularly for CCL2 and CCL7, our data in DT-treated DTR^{+} mice demonstrated a reduction after specific depletion of LCs, while the total numbers of DN- and DP-DCs remained unchanged. Perhaps this is just because more LCs than DP-DCs migrate to the dLN following ECTV infection. LCs are well known for their superior ability to prime the adaptive immune response, as decades of research have demonstrated their ability to prime CD8^{+} T cells (Clausen and Stoitzner, 2015; Doebel et al., 2017; Kaplan, 2010; Merad et al., 2008), and for their importance in CD4^{+} T follicular helper cell activation in germinal center reactions, which are necessary for high-affinity antibody responses (Zimara et al., 2014). It is also known that LCs are important as APCs for skin-resident T cells and the recruitment of other immune cells, such as NK cells to the skin (West and Bennett, 2018). Our new study demonstrates that LCs also play a key role in the recruitment of iMOs and NK cells to the dLN in response to infection and optimal intrinsic resistance to a highly lethal viral disease. This study complements our previous work showing that infected skin-derived DCs activate NK

cells and ILC1s already present in the dLN through NKG2D to produce the early IFN-γ that recruited iMOs need to secrete CXCL9 to recruit circulating NK cells through CXCR3 (Wong et al., 2018). Our data show that LCs have high expression of the NKG2D ligand MULT1 and may be the critical subset in mediating the early source of NKG2D-induced IFN-γ. Future studies should focus on identifying the signaling pathways that trigger the recruitment of MHC class II^{hi} DCs from the skin to the dLN, as well as on elucidating the other roles that MHC class II^{hi} DCs play in the early immune response in the dLN. Overall, our study highlights the critical role that MHC class II^{hi} DCs in general and LCs in particular play in the dLN as the architects of the early IIR to a lethal viral infection.

STAR★METHODS

Detailed methods are provided in the online version of this paper and include the following:

- KEY RESOURCES TABLE
- LEAD CONTACT AND MATERIALS AVAILABILITY
- EXPERIMENTAL MODEL AND SUBJECT DETAILS
- METHOD DETAILS
  - Viruses and Infection
  - Injections and Cell Depletions
  - Flow Cytometry
  - Illumination of Ubc-PA-GFP Mice
  - RNA Preparation and RT-qPCR
- QUANTIFICATION AND STATISTICAL ANALYSIS
- DATA AND CODE AVAILABILITY

SUPPLEMENTAL INFORMATION

Supplemental Information can be found online at https://doi.org/10.1016/j.celrep.2019.10.118.

ACKNOWLEDGMENTS

We thank Lingjuan Tang and Ni Meng for technical assistance and Jennifer Wilson for editing the manuscript. This research was supported by National Institute of Allergy and Infectious Diseases (NIAID) grants R0AI110457 and R01AI065544 and National Institute on Aging (NIA) grant R01AG048602 to L.J.S. and grant F32AI129352 to E.W. Research reported in this publication utilized the flow cytometry and laboratory animal facilities at Sidney Kimmel Cancer Center at Jefferson Health and was supported by the National Cancer Institute of the National Institutes of Health (NIH) under award number P30CA056036. Publication was made possible in part by support from the Thomas Jefferson University + Philadelphia University Open Access Fund. The graphical abstract was created with BioRender.com.

AUTHOR CONTRIBUTIONS

E.W. and L.J.S. conceived and designed experiments, analyzed results, and co-wrote the paper. E.W. performed most of the experiments. L.J.S. conceived the initial idea and supervised the work. B.M., C.S., and M.F. helped with some of the experiments, and R.-H.X. designed and performed some experiments.

DECLARATION OF INTERESTS

The authors declare no competing interests.

Received: May 18, 2019
Revised: September 17, 2019
Accepted: October 29, 2019
Published: December 3, 2019

REFERENCES

Allan, R.S., Waithman, J., Bedoui, S., Jones, C.M., Villadangos, J.A., Zhan, Y., Lew, A.M., Shortman, K., Heath, W.R., and Carbone, F.R. (2006). Migratory dendritic cells transfer antigen to a lymph node-resident dendritic cell population for efficient CTL priming. Immunity *25*, 153–162.

Alvarez, D., Vollmann, E.H., and von Andrian, U.H. (2008). Mechanisms and consequences of dendritic cell migration. Immunity *29*, 325–342.

Bedoui, S., and Greyer, M. (2014). The role of dendritic cells in immunity against primary herpes simplex virus infections. Front. Microbiol. *5*, 533.

Bennett, C.L., Noordegraaf, M., Martina, C.A.E., and Clausen, B.E. (2007). Langerhans cells are required for efficient presentation of topically applied hapten to T cells. J. Immunol. *179*, 6830–6835.

Bobr, A., Olvera-Gomez, I., Igyártó, B.Z., Haley, K.M., Hogquist, K.A., and Kaplan, D.H. (2010). Acute ablation of Langerhans cells enhances skin immune responses. J. Immunol. *185*, 4724–4728.

Bogoslowski, A., Butcher, E.C., and Kubes, P. (2018). Neutrophils recruited through high endothelial venules of the lymph nodes via PNAd intercept disseminating *Staphylococcus aureus*. Proc. Natl. Acad. Sci. USA *115*, 2449–2454.

Burns, D.L. (1988). Subunit structure and enzymic activity of pertussis toxin. Microbiol. Sci. *5*, 285–287.

Chapman, J.L., Nichols, D.K., Martinez, M.J., and Raymond, J.W. (2010). Animal models of orthopoxvirus infection. Vet. Pathol. *47*, 852–870.

Clausen, B.E., and Stoitzner, P. (2015). Functional specialization of skin dendritic cell subsets in regulating T cell responses. Front. Immunol. *6*, 534.

Conrady, C.D., Drevets, D.A., and Carr, D.J.J. (2010). Herpes simplex type I (HSV-1) infection of the nervous system: is an immune response a good thing? J. Neuroimmunol. *220*, 1–9.

Desai, P., Tahiliani, V., Abboud, G., Stanfield, J., and Salek-Ardakani, S. (2018). Batf3-dependent dendritic cells promote optimal CD8 T cell responses against respiratory poxvirus infection. J. Virol. *92*, 80.

Doebel, T., Voisin, B., and Nagao, K. (2017). Langerhans cells—the macrophage in dendritic cell clothing. Trends Immunol. *38*, 817–828.

Fang, M., and Sigal, L.J. (2005). Antibodies and CD8+ T cells are complementary and essential for natural resistance to a highly lethal cytopathic virus. J. Immunol. *175*, 6829–6836.

Fang, M., Lanier, L.L., and Sigal, L.J. (2008). A role for NKG2D in NK cell-mediated resistance to poxvirus disease. PLoS Pathog. *4*, e30.

Fang, M., Orr, M.T., Spee, P., Egebjerg, T., Lanier, L.L., and Sigal, L.J. (2011). CD94 is essential for NK cell-mediated resistance to a lethal viral disease. Immunity *34*, 579–589.

Farrell, H.E., Davis-Poynter, N., Bruce, K., Lawler, C., Dolken, L., Mach, M., and Stevenson, P.G. (2015). Lymph node macrophages restrict murine cytomegalovirus dissemination. J. Virol. *89*, 7147–7158.

Farrell, H.E., Lawler, C., Tan, C.S.E., MacDonald, K., Bruce, K., Mach, M., Davis-Poynter, N., and Stevenson, P.G. (2016). Murine cytomegalovirus exploits olfaction to enter new hosts. MBio *7*, e00251–e16.

Flint, J., Racaniello, V.R., Rall, G.F., and Skalka, A.M. (2015). Principles of Virology, Fourth Edition Bundle (American Society of Microbiology).

Fukunaga, A., Khaskhely, N.M., Sreevidya, C.S., Byrne, S.N., and Ullrich, S.E. (2008). Dermal dendritic cells, and not Langerhans cells, play an essential role in inducing an immune response. J. Immunol. *180*, 3057–3064.

Garcia, Z., Lemaitre, F., van Rooijen, N., Albert, M.L., Levy, Y., Schwartz, O., and Bousso, P. (2012). Subcapsular sinus macrophages promote NK cell accumulation and activation in response to lymph-borne viral particles. Blood *120*, 4744–4750.

Gordon, S., and Taylor, P.R. (2005). Monocyte and macrophage heterogeneity. Nat. Rev. Immunol. *5*, 953–964.

He, Y., and Falo, L.D. (2006). Induction of T cell immunity by cutaneous genetic immunization with recombinant lentivector. Immunol. Res. *36*, 101–117.

Helft, J., Manicassamy, B., Guermonprez, P., Hashimoto, D., Silvin, A., Agudo, J., Brown, B.D., Schmolke, M., Miller, J.C., Leboeuf, M., et al. (2012). Cross-presenting CD103+ dendritic cells are protected from influenza virus infection. J. Clin. Invest. *122*, 4037–4047.

Henri, S., Poulin, L.F., Tamoutounour, S., Ardouin, L., Guilliams, M., de Bovis, B., Devilard, E., Viret, C., Azukizawa, H., Kissenpfennig, A., and Malissen, B. (2010). CD207+ CD103+ dermal dendritic cells cross-present keratinocyte-derived antigens irrespective of the presence of Langerhans cells. J. Exp. Med. *207*, 189–206.

Hildner, K., Edelson, B.T., Purtha, W.E., Diamond, M., Matsushita, H., Kohyama, M., Calderon, B., Schraml, B.U., Unanue, E.R., Diamond, M.S., et al. (2008). Batf3 deficiency reveals a critical role for CD8alpha+ dendritic cells in cytotoxic T cell immunity. Science *322*, 1097–1100.

Hume, D.A. (2008). Macrophages as APC and the dendritic cell myth. J. Immunol. *181*, 5829–5835.

Iannacone, M., Moseman, E.A., Tonti, E., Bosurgi, L., Junt, T., Henrickson, S.E., Whelan, S.P., Guidotti, L.G., and von Andrian, U.H. (2010). Subcapsular sinus macrophages prevent CNS invasion on peripheral infection with a neurotropic virus. Nature *465*, 1079–1083.

Jacoby, R.O., Bhatt, P.N., and Brownstein, D.G. (1989). Evidence that NK cells and interferon are required for genetic resistance to lethal infection with ectromelia virus. Arch. Virol. *108*, 49–58.

Junt, T., Moseman, E.A., Iannacone, M., Massberg, S., Lang, P.A., Boes, M., Fink, K., Henrickson, S.E., Shayakhmetov, D.M., Di Paolo, N.C., et al. (2007). Subcapsular sinus macrophages in lymph nodes clear lymph-borne viruses and present them to antiviral B cells. Nature *450*, 110–114.

Kaminsky, L.W., Sei, J.J., Parekh, N.J., Davies, M.L., Reider, I.E., Krouse, T.E., and Norbury, C.C. (2015). Redundant function of plasmacytoid and conventional dendritic cells is required to survive a natural virus infection. J. Virol. *89*, 9974–9985.

Kaplan, D.H. (2010). In vivo function of Langerhans cells and dermal dendritic cells. Trends Immunol. *31*, 446–451.

Kaplan, D.H., Jenison, M.C., Saeland, S., Shlomchik, W.D., and Shlomchik, M.J. (2005). Epidermal langerhans cell-deficient mice develop enhanced contact hypersensitivity. Immunity *23*, 611–620.

Karimian, G., Buist-Homan, M., Faber, K.N., and Moshage, H. (2012). Pertussis toxin, an inhibitor of G(αi) PCR, inhibits bile acid- and cytokine-induced apoptosis in primary rat hepatocytes. PLoS ONE *7*, e43156.

Karupiah, G., Fredrickson, T.N., Holmes, K.L., Khairallah, L.H., and Buller, R.M. (1993). Importance of interferons in recovery from mousepox. J. Virol. *67*, 4214–4226.

Kashem, S.W., Igyártó, B.Z., Gerami-Nejad, M., Kumamoto, Y., Mohammed, J.A., Jarrett, E., Drummond, R.A., Zurawski, S.M., Zurawski, G., Berman, J., et al. (2015). Candida albicans morphology and dendritic cell subsets determine T helper cell differentiation. Immunity *42*, 356–366.

Kissenpfennig, A., Henri, S., Dubois, B., Laplace-Builhé, C., Perrin, P., Romani, N., Tripp, C.H., Douillard, P., Leserman, L., Kaiserlian, D., et al. (2005). Dynamics and function of Langerhans cells in vivo: dermal dendritic cells colonize lymph node areas distinct from slower migrating Langerhans cells. Immunity *22*, 643–654.

Lee, H.K., Zamora, M., Linehan, M.M., Iijima, N., Gonzalez, D., Haberman, A., and Iwasaki, A. (2009). Differential roles of migratory and resident DCs in T cell priming after mucosal or skin HSV-1 infection. J. Exp. Med. *206*, 359–370.

Malissen, B., Tamoutounour, S., and Henri, S. (2014). The origins and functions of dendritic cells and macrophages in the skin. Nat. Rev. Immunol. *14*, 417–428.

Melzi, E., Caporale, M., Rocchi, M., Martín, V., Gamino, V., di Provvido, A., Marruchella, G., Entrican, G., Sevilla, N., and Palmarini, M. (2016). Follicular dendritic cell disruption as a novel mechanism of virus-induced immunosuppression. Proc. Natl. Acad. Sci. USA *113*, E6238–E6247.

Merad, M., Ginhoux, F., and Collin, M. (2008). Origin, homeostasis and function of Langerhans cells and other langerin-expressing dendritic cells. Nat. Rev. Immunol. *8*, 935–947.

Merad, M., Sathe, P., Helft, J., Miller, J., and Mortha, A. (2013). The dendritic cell lineage: ontogeny and function of dendritic cells and their subsets in the steady state and the inflamed setting. Annu. Rev. Immunol. *31*, 563–604.

Metlay, J.P., Witmer-Pack, M.D., Agger, R., Crowley, M.T., Lawless, D., and Steinman, R.M. (1990). The distinct leukocyte integrins of mouse spleen dendritic cells as identified with new hamster monoclonal antibodies. J. Exp. Med. *171*, 1753–1771.

Mildner, A., and Jung, S. (2014). Development and function of dendritic cell subsets. Immunity *40*, 642–656.

Moll, H., Flohé, S., and Röllinghoff, M. (1995). Dendritic cells in Leishmania major-immune mice harbor persistent parasites and mediate an antigen-specific T cell immune response. Eur. J. Immunol. *25*, 693–699.

Murphy, K.M. (2013). Transcriptional control of dendritic cell development. Adv. Immunol. *120*, 239–267.

Parker, A.K., Parker, S., Yokoyama, W.M., Corbett, J.A., and Buller, R.M.L. (2007). Induction of natural killer cell responses by ectromelia virus controls infection. J. Virol. *81*, 4070–4079.

Remakus, S., Rubio, D., Ma, X., Sette, A., and Sigal, L.J. (2012). Memory CD8+ T cells specific for a single immunodominant or subdominant determinant induced by peptide-dendritic cell immunization protect from an acute lethal viral disease. J. Virol. *86*, 9748–9759.

Roscoe, F., Xu, R.H., and Sigal, L.J. (2012). Characterization of ectromelia virus deficient in EVM036, the homolog of vaccinia virus F13L, and its application for rapid generation of recombinant viruses. J. Virol. *86*, 13501–13507.

Rubio, D., Xu, R.H., Remakus, S., Krouse, T.E., Truckenmiller, M.E., Thapa, R.J., Balachandran, S., Alcamí, A., Norbury, C.C., and Sigal, L.J. (2013). Cross-talk between the type 1 interferon and nuclear factor kappa B pathways confers resistance to a lethal virus infection. Cell Host Microbe *13*, 701–710.

Sei, J.J., Haskett, S., Kaminsky, L.W., Lin, E., Truckenmiller, M.E., Bellone, C.J., Buller, R.M., and Norbury, C.C. (2015). Peptide-MHC-I from endogenous antigen outnumber those from exogenous antigen, irrespective of APC phenotype or activation. PLoS Pathog. *11*, e1004941.

Sigal, L.J. (2016). The pathogenesis and immunobiology of mousepox. In Advances in Immunology (Elsevier), pp. 251–276.

Stoitzner, P., Pfaller, K., Stössel, H., and Romani, N. (2002). A close-up view of migrating Langerhans cells in the skin. J. Invest. Dermatol. *118*, 117–125.

Tiberio, L., Del Prete, A., Schioppa, T., Sozio, F., Bosisio, D., and Sozzani, S. (2018). Chemokine and chemotactic signals in dendritic cell migration. Cell. Mol. Immunol. *15*, 346–352.

Torti, N., Walton, S.M., Murphy, K.M., and Oxenius, A. (2011). Batf3 transcription factor-dependent DC subsets in murine CMV infection: differential impact on T-cell priming and memory inflation. Eur. J. Immunol. *41*, 2612–2618.

Tussiwand, R., Lee, W.L., Murphy, T.L., Mashayekhi, M., Kc, W., Albring, J.C., Satpathy, A.T., Rotondo, J.A., Edelson, B.T., Kretzer, N.M., et al. (2012). Compensatory dendritic cell development mediated by BATF-IRF interactions. Nature *490*, 502–507.

Victora, G.D., Schwickert, T.A., Fooksman, D.R., Kamphorst, A.O., Meyer-Hermann, M., Dustin, M.L., and Nussenzweig, M.C. (2010). Germinal center dynamics revealed by multiphoton microscopy with a photoactivatable fluorescent reporter. Cell *143*, 592–605.

Virgin, H.W. (2005). Immune regulation of viral infection and vice versa. Immunol. Res. *32*, 293–315.

Waithman, J., Zanker, D., Xiao, K., Oveissi, S., Wylie, B., Ng, R., Tögel, L., and Chen, W. (2013). Resident CD8(+) and migratory CD103(+) dendritic cells control CD8 T cell immunity during acute influenza infection. PLoS ONE *8*, e66136.

Wallace, G.D., and Buller, R.M. (1985). Kinetics of ectromelia virus (mousepox) transmission and clinical response in C57BL/6j, BALB/cByj and AKR/J inbred mice. Lab. Anim. Sci. *35*, 41–46.

Wallace, G.D., Buller, R.M., and Morse, H.C., 3rd. (1985). Genetic determinants of resistance to ectromelia (mousepox) virus-induced mortality. J. Virol. *55*, 890–891.

West, H.C., and Bennett, C.L. (2018). Redefining the role of Langerhans cells as immune regulators within the skin. Front. Immunol. *8*, 1941.

Wong, E., Xu, R.H., Rubio, D., Lev, A., Stotesbury, C., Fang, M., and Sigal, L.J. (2018). Migratory dendritic cells, group 1 innate lymphoid cells, and inflammatory monocytes collaborate to recruit NK cells to the virus-infected lymph node. Cell Rep. *24*, 142–154.

Xu, R.H., Fang, M., Klein-Szanto, A., and Sigal, L.J. (2007). Memory CD8+ T cells are gatekeepers of the lymph node draining the site of viral infection. Proc. Natl. Acad. Sci. USA *104*, 10992–10997.

Xu, R.H., Cohen, M., Tang, Y., Lazear, E., Whitbeck, J.C., Eisenberg, R.J., Cohen, G.H., and Sigal, L.J. (2008). The orthopoxvirus type I IFN binding protein is essential for virulence and an effective target for vaccination. J. Exp. Med. *205*, 981–992.

Xu, R.H., Remakus, S., Ma, X., Roscoe, F., and Sigal, L.J. (2010). Direct presentation is sufficient for an efficient anti-viral CD8+ T cell response. PLoS Pathog. *6*, e1000768.

Xu, R.H., Wong, E.B., Rubio, D., Roscoe, F., Ma, X., Nair, S., Remakus, S., Schwendener, R., John, S., Shlomchik, M., and Sigal, L.J. (2015). Sequential activation of two pathogen-sensing pathways required for type I interferon expression and resistance to an acute DNA virus infection. Immunity *43*, 1148–1159.

Zimara, N., Florian, C., Schmid, M., Malissen, B., Kissenpfennig, A., Männel, D.N., Edinger, M., Hutchinson, J.A., Hoffmann, P., and Ritter, U. (2014). Langerhans cells promote early germinal center formation in response to Leishmania-derived cutaneous antigens. Eur. J. Immunol. *44*, 2955–2967.

STAR★METHODS

KEY RESOURCES TABLE

REAGENT or RESOURCE	SOURCE	IDENTIFIER
Antibodies		
BV785-CD3ε (Clone 145-2C11)	Biolegend	Cat#100302; RRID: AB_312667
BV711-CD8α (Clone 53-6.7)	Biolegend	Cat#100759; RRID: AB_2563510
APC/Cy7-CD11b (Clone M1/70)	Biolegend	Cat#101226; RRID: AB_830642
BV-421-Gr-1 (Clone RB6-8C5)	Biolegend	Cat#108433; RRID: AB_10900232
PE/Cy7-CD11c (Clone N418)	Biolegend	Cat#117317; RRID: AB_493569
FITC-CD45 (Clone I3/2.3)	Biolegend	Cat#147709; RRID: AB_2563541
PerCP/Cy5.5-IA^b (Clone AF6-120.1)	Biolegend	Cat#116415; RRID: AB_1953308
PerCP/Cy5.5-CD103 (Clone 2E7)	Biolegend	Cat#121416; RRID: AB_2128621
APC-CD207 (Clone 4C7)	Biolegend	Cat#144205; RRID: AB_2561997
PE-CD64 (Clone X54-5/7.1)	Biolegend	Cat#139303; RRID: AB_10613467
APC-F4/80 (Clone BM8)	Biolegend	Cat#123115; RRID: AB_893493
BV605-NK1.1 (PK136)	Biolegend	Cat#108739; RRID: AB_2562273
BUV395-CD4 (Clone GK1.5)	BD Biosciences	Cat#563790; RRID not available
BUV395-CD19 (Clone 1D3)	BD Biosciences	Cat#563557; RRID not available
Virus Strains		
Ectromelia virus Moscow strain	ATCC	Cat#VR-1374
Chemicals, Peptides, and Recombinant Proteins		
Pertussis toxin from *Bortedella pertussis*	Sigma	Cat#P7208
Diphtheria toxin derived from *Corynebacterium diphtheriae*	EMD Millipore	Cat#322326
Critical Commercial Assays		
RNeasy Mini Kit	QIAGEN	Cat#74104
High Capacity cDNA Reverse Transcription Kit	Thermo Fisher	Cat#4368814
iTaq Universal SYBR Green supermix	BioRad	Cat#1725124
Experimental Models: Cell Lines		
BS-C-1	ATCC	Cat#CCL-26
Experimental Models: Organisms/Strains		
C57BL/6N (B6)	Charles River	Cat#027
B6.129S(C)-*Batf3*^{tm1Kmm}/J	Jackson Laboratories	Cat#013758
B6.Cg-*Ptprc*^{a} Tg(UBC-PA-GFP)1Mnz/J	Gift from Gabriel Victora - Rockefeller University	NA
HuLangerin-DTR	Gift from Daniel Kaplan – University of Pittsburg	NA
Oligonucleotides		
See Table S1		
Software and Algorithms		
FlowJo V.10.1	TreeStar	https://wwws.flowjo.com
Prism 6	GraphPad	https://www.graphpad.com/scientific-software/prism
Illustrator CS5	Adobe	www.adobe.com/products/illustrator.html

LEAD CONTACT AND MATERIALS AVAILABILITY

This study did not generate new unique reagents. Further information and/or requests for resources and reagents should be directed to and will be fulfilled by the Lead Contact, Luis Sigal (luis.sigal@jefferson.edu).

EXPERIMENTAL MODEL AND SUBJECT DETAILS

All the procedures involving mice were carried out in strict accordance with the recommendations in the Eight Edition of the Guide for the Care and Use of Laboratory Animals of the National Research Council of the National Academies. All protocols were approved by Thomas Jefferson University's Institutional Animal Care and Use Committee. All mice used in experiments were 6-12 weeks old and males and females were both used. Colonies were bred at Thomas Jefferson University under specific pathogen free conditions. Animals were housed in a controlled environment with 12-hour day/night cycle with optimal temperature and fed rodent chow *ad libitum*. C57BL/6 (B6) mice were purchased from Charles River. B6.129S(C)-*Batf3*^{tm1Kmm}/J (*Batf3*$^{-/-}$) mice were purchased from Jackson Laboratories. Breeder mice expressing photoactivatable green fluorescence protein under the mouse Ubiquitin C promoter (*Ubc*-PA-GFP mice) were a gift from Dr. Gabriel Victora (Rockefeller University, New York, NY). Breeder mice expressing the human diphtheria toxin receptor under the human Langerin (CD207) promoter (CD207-DTR mice) mice were a gift from Dr. Daniel Kaplan (University of Pittsburgh, Pittsburg, PA).

METHOD DETAILS

Viruses and Infection

Virus stocks, including ECTV-Moscow strain (ATCC VR-1374), ECTV-EGFP (Fang et al., 2008), and ECTV-dsRED (Roscoe et al., 2012) were propagated in tissue culture as previously described (Xu et al., 2008). Briefly, new stocks were expanded by infecting BALB/c mice with 3000 PFU of ECTV in the footpad. Seven days p.i., the spleen and liver were removed and homogenized in 20 mL of RPMI using a tissue homogenizer. The solid material was pelleted by centrifugation, and the supernatant was stored in aliquots at −80°C. Virus titers in ECTV stocks were determined by plaque assays on BSC-1 cells. Briefly, 10-fold serial dilutions of the stocks in 0.5 mL of RPMI 2.5 were used to infect confluent BSC-1 cells in 6-well plates (2 wells/dilution) for 1 h. Two milliliters of fresh RPMI 2.5 were then added, and the cells were incubated at 37°C for 5 days. After this time, the medium was aspirated and the cells fixed and stained for 10 min with 0.1% crystal violet and 20% ethanol in water. The fix/stain solution was subsequently aspirated, the cells air-dried, the plaques counted, and the PFU per milliliter in stocks were calculated accordingly.

Mice were infected in the footpad with 3,000 plaque forming units (PFUs) ECTV (ECTV-WT, ECTV-dsRED, or ECTV-EGFP) in 30 μL PBS using a 1 mL syringe and a 27 g needle. For the determination of survival, mice were monitored daily for signs of disease (lethargy, weight loss, skin rash, ruffled hair, and eye secretions) and to avoid unnecessary suffering, mice were euthanized and counted as dead when imminent death was certain as determined by lack of activity and unresponsiveness to touch. Euthanasia was according to the 2013 edition of the AVMA Guideline for the Euthanasia of Animals.

For virus titers, the entire spleen or portions of the liver were homogenized in RPMI using a Tissue Lyser (QIAGEN). Virus titers were determined on BSC-1 cells as before (Xu et al., 2008). Briefly, infected spleens and livers were prepared as single-cell suspensions through disruption between two frosted glass slides. 10-fold serial dilutions of the stocks in 0.5 mL of RPMI 2.5 were used to infect confluent BSC-1 cells in 24-well plates for 2 h. The supernatant was aspirated followed by the addition of 500 μl of carboxymethyl cellulose, and the cells were incubated at 37°C for 5 days. After this time, the medium was aspirated and the cells fixed with 5% formaldehyde and stained for 10 min with 0.1% crystal violet and 20% ethanol in water. The fix/stain solution was subsequently aspirated, the cells air-dried, the plaques counted, and the PFU per milliliter in stocks were calculated accordingly.

Injections and Cell Depletions

To block the migration of skin-derived cells from the footpad to dLN, B6 mice were injected with 200 ng of pertussis toxin derived from *Bordetella pertussis* (Sigma) or control PBS in the footpad 1 d before and 1 d after infection with ECTV. To deplete LCs, CD207-DTR mice were injected IP with 500 ng of diphtheria toxin derived from *Corynebacterium diphtheriae* (EMD Millipore) 1 d before and 1 d after infection with ECTV. Efficient depletion of Langerhans cells was confirmed by flow cytometry using mAbs CD11c, MHC-II, CD103 and CD207 in the LN at 1 d after the second depletion.

Flow Cytometry

Flow cytometry was performed as previously described (Xu et al., 2008). To obtain single-cell suspensions, LNs were first incubated in Liberase TM (1.67 Wünsch units/mL) (Sigma) in PBS with 25 mM HEPES for 30 min at 37°C before adding PBS with 25 mM HEPES + 10% FBS to halt the digestion process, followed by mechanical disruption of the tissue through a 70-μm filter. Cells were washed once with FACS buffer (PBS with 1% BSA + 0.1% sodium azide) before surface staining. For analysis, samples were acquired using either a BD LSR II flow cytometer or a BD Fortessa flow cytometer (BD Biosciences), and data were analyzed with FlowJo software (TreeStar). For cell sorting, samples were acquired with a BD FACS Aria III sorter (BD Bioscience).

Illumination of Ubc-PA-GFP Mice

Ubc-PA-GFP mice were anesthetized with 3% isoflurane and one or both hind feet were illuminated for 30 min with a 415 nm laser light source (Prizmatix). The illuminated mice were rested for 4 h before they were infected with ECTV.

RNA Preparation and RT-qPCR

Total RNA from LNs or sorted cells (10^4-10^5 cells) was obtained with the RNeasy Mini Kit (QIAGEN) according to manufacturer's instructions and as previously described (Rubio et al., 2013; Xu et al., 2015). 1 μg of total RNA samples were synthesized with High Capacity cDNA Reverse Transcription Kit (Life Technologies) according to manufacturer's instructions. qPCR was performed as before (Rubio et al., 2013; Xu et al., 2015) using primers as listed in the Key Resources Table. 1 ng of cDNA from each sample was run in 20 ul reaction using iTaq Universal SYBR Green universal PCR supermix (Bio-Rad). Reactions were performed in a Bio-Rad CFX96. Ratios of mRNA levels to control values were calculated using the ΔCt method at a threshold of 0.02. All data were normalized to control GAPDH. PCR conditions used: hold for 10 min at 95°C, followed by 40 cycles of 15 s at 95°C and 60 s at 60°C.

QUANTIFICATION AND STATISTICAL ANALYSIS

Data were analyzed with Prism 6 software (GraphPad Software). For survival we used the Log-rank (Mantel-Cox). For other experiments ANOVA with Tukey correction for multiple comparisons or Student's t test were used as applicable. In all figures, *$p < 0.05$, **$p < 0.01$, ***$p < 0.001$, ****$p < 0.001$.

DATA AND CODE AVAILABILITY

This study did not generate any datasets or code.